Advances in Astronomy and Space Physics, **8**, 16-23 (2018) doi: 10.17721/2227-1481.8.16-23

The primordial helium abundance determination using multicomponent photoionization modelling of low-metallicity H II regions

I. O. Koshmak[*], *B. Ya. Melekh*[†]

Department of Astrophysics, Ivan Franko National University of Lviv, 8 Kyryla & Mephodiya str., Lviv, Ukraine

The method for the multicomponent photoionization modelling (MPhM) of low-metallicity H II regions surrounding the starburst region was developed. The internal structure of the H II region has been determined using the evolutionary modelling of the superwind bubble surrounding the star-forming region. Models of Chevalier and Clegg (1985) and Weaver et al. (1977) have been used to determine the radial distribution of the gas density, the velocity of gas layers, and the temperature within internal components (the region of the superwind free expansion and the cavity, respectively). The chemical abundances in region of the superwind free expansion were obtained from the evolutionary population synthesis with including of rotating stars. The chemical abundances within cavity were defined by averaging over mass the chemical compositions of mixture of the abundances of gas from superwind and ones within outer component, because of gas evaporation from external component into the cavity. External components of our models describe a high-density, thin shell of gas formed by superwind shock and a typical undisturbed hydrodynamically H II region, respectively. Evolutionary grids of multicomponent low-metallicity models are calculated. A comparative analysis of the results of their calculation with the observed data has been carried out. The ionic abundances averaged over modelling volume as well as chemical composition assumed in models were used to derive the new expressions for ionization-correction factors that were used to redetermine the chemical compositions of 88 H II regions in blue compact dwarf galaxies. It must be noticed that we used for this propose the ionic abundances obtained by Izotov et al. (2007). In result the primordial helium abundance and its enrichment during stellar chemical evolution of matter were determined.

Key words: ISM: H II regions, bubbles, evolution – galaxies: starburst

INTRODUCTION

The low-metallicity H II regions in blue compact dwarf galaxies (BCDG) are usually used to determine the primordial helium abundance and its enrichment during stellar chemical evolution of matter (see i.e. [8, 9, 30]). It is because they are characterized by lowest metallicity from the all types of nebular objects, and, on the other hand, the primordial helium synthesis has been occurred during Big Bang Nucleosynthesis epoch, when heavy elements were not synthesized (metallicity $Z = 0$).

To determine the chemical composition of H II regions in BCDG the ionic abundances, obtained during nebular diagnostics, as well as ionization correction factors (ICFs – expressions to take into account the unobserved ionization stages of the chemical elements) are used in most cases. The ICFs are derived mainly basing on the grid of photoionization models (PhMs) calculated for this type of nebular objects (see i.e. [6–8, 30]).

Thus, the PhMs should represent, as far as it possible on the present day, the physical conditions in real H II regions. Particularly, during such modelling it is important to describe the internal structure of H II region in BCDG. In most of previous works on the photoionization modelling of low-metallicity H II regions (see i.e. [6, 28]) the possible presence of internal structure of nebular region driven by superwind blowing out from central star-forming region was neglected.

In our previous investigations [16, 19] we have calculated the multicomponent photoionization models (MPhMs) of the H II regions and it was shown that, under certain circumstances, bubble-like structures formed by the stellar superwind can lead to a lack of quanta in the energy distribution in the spectrum of the ionizing radiation that ionizes the surrounding hydrodynamically undisturbed H II region. In [16], the gas density was assumed to be different for each

[*] ihorkoshmak@gmail.com
[†] bmelekh@gmail.com

component of the bubble, but it was assumed to be constant over volume of each of components. More complex multicomponent models were developed by us in [19], where theory of bubble-structure evolution, proposed by Weaver & Castor [31], was used to describe the density and temperature distributions within the superwind region (SWR).

In [14, 15] we have included to our MPhMs the dust grains. The direct interaction of gas and dust appears in the photoelectric effect of dust grains leading to dust cooling and gas heating, and, on the other hand, the absorption of UV quanta by dust and gas-dust collisions leading to the dust heating and gas cooling.

Also, the assumption of the presence of a complex internal structure within the H II region, which we have taken into account in our simulations and described in [13], makes it possible to explain the presence of high excitation lines of He II 4686 Å and [Ne V] 3626 Å in observed spectra of H II regions in BCDGs [30].

In present work we used the model of Chevalier and Clegg [3] to define the temperature distribution in the superwind free expansion region (it is the first component in our simulations). Also, we reduced the number of free parameters in our models making the modelling process more self-consistent. The simulation stops if the pressure at the external boundary of the bubble drops to the one at the inner edge of surrounding H II region. According to our assumption such situation indicates the cease of expansion of the internal structure. After that most probably the adopted SWR structure begins to decay due to the hydrodynamic instabilities. Thus, we were able to estimate the upper limit of the bubble lifetime by modelling.

To determine the new expressions for ICFs we used ionic abundances, obtained during calculation of MPhMs and averaged over volumes of outer bubble component as well as outer hydrodynamically undisturbed H II (the most of observed emission lines), as well as the arises in these components), and chemical compositions adopted in MPhMs. These expressions as well as ionic abundances of 88 objects from [8–12], were used for re-determination of the chemical compositions in H II regions in BCDGs. With these chemical compositions the primordial helium abundance Y_p and its enrichment during stellar chemical evolution of matter were obtained.

SUPEWIND BUBBLE MODEL

The main source of the ionizing radiation in our models is the central star-forming region. The superwind blowing out from this region forms a shock-wave that compress the surrounding nebular gas and forms the thin dense shell [31]. The reverse shock-wave thermalizes the rarefied gas in the cavity [31]. As a result, the superwind cavity emits thermal radiation at very high temperature (sometimes it reaches more than 10^6 K). The complex structure of the surrounding nebular environment we divided into four following main components (see Fig. 1):

(1) The first component is the superwind, freely expanding from the star-forming region.

(2) The second component is the hot rarefied gas of the superwind cavity.

(3) The third component is the high-density shell compressed by the superwind shock wave.

(4) The fourth component is the normal H II region.

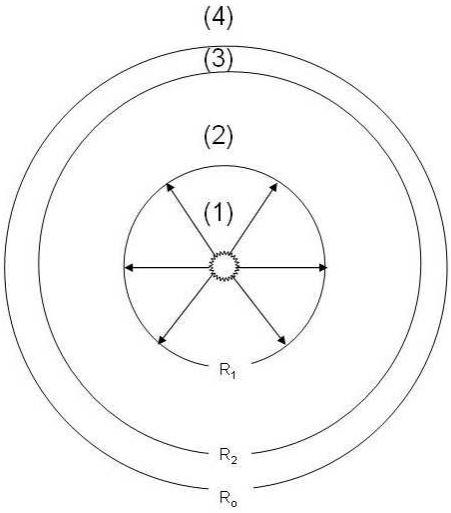

Fig. 1: Superwind bubble structure.

THE EVOLUTIONARY POPULATION MODELS OF STARBURST

In the first component, which is the closest to the starburst knot, the incoming Lyman continuum (Lyc) spectrum is defined by stars inside the central star-forming region. The stars formation occurs in bursts (assuming that all the stars emerged at the initial time). We calculated starburst using evolutionary synthesis code `Starburst 99` [17]. The total fixed mass of the stars was assumed to be of (10^4, 10^5, 10^6, 10^7, 10^8) $M_\odot$; exponents of the Kroupa initial mass functions of stars are of 1.3 and 2.3 in the range of stellar masses $(0.1 \dots 0.5)$ $M_\odot$ and of $(0.5 \dots 100)$ $2M_\odot$, correspondingly. Evolutionary tracks `Geneva v40` (the starting rotation rate of the WR-stars is 40% of the parabolic velocity on zero age at main sequence) for the metallicity of 0.001 were used. The Maeder wind model [26, 27] was adopted. We start simulation from age of 10000 years until 20 Myr with timeline step of 10000 years. The grid is based on Pauldrach/Hillier stellar atmosphere

models [21]. The microturbulence velocity in the atmospheres of red giants, which was used to calculate the near infrared spectrum, is set to 3 km/s.

As a result of calculations, the evolution of the following characteristics was investigated: Lyc-spectrum of star-forming region, total number of the ionizing quanta, chemical composition of elements escaping into the surrounding region due to the superwind and supernova explosions, starburst rate of mass loss to superwind $\dot{M}_{\rm w}$, total mass $M_{sb} = \int_0^{age} \dot{M}_{\rm w} dt$ of inner SWR components 1 and 2, mechanical luminosity L_w.

MULTICOMPONENT PHOTOIONIZAION MODELLING

Each of modelling components is a separate spherically symmetrical photoionization model. The photoionization in each of these components is caused by two kinds of radiation quanta:

1. Quanta of direct radiation from the ionization source (star); He II not absorbed in the previous component.
2. Quanta of diffuse radiation emitted in the previous and present components on the way from inside to outside, the simulated layer (the diffuse radiation was calculated in the outward only approximation [29]).

Code `Cloudy 08.00` developed by G. Ferland [5] was used to calculate the photoionization models. We modified its kernel in order to implement a multicomponent modelling and developed a driver for this code with purpose to organize the MPhMs grid calculation and storage of the results.

Thus, the grid of 4-component MPhMs was calculated with the following free parameters:

1. The age of the starburst knot ($t = 1 \ldots 20$ Myr).
2. The density in component 4 ($n_0 = 0.05, 1, 10, 50, 100\,{\rm cm}^{-3}$).
3. The chemical compositions in the 3rd and 4th components.

Such grid was calculated separately for the every mass of star-forming region mentioned above.

The chemical compositions inside the component 1 were obtained using the evolutionary population synthesis code `Starburst 99` [17], while metallicity of outer components 3 and 4 were adopted in the metallicity range corresponding to the oxygen abundance within range of $12+\lg({\rm O/H}) = 7.1-8.2$. Gas abundances of Ne/H, S/H, Ar/H and Fe/H in the 3rd and 4th components of the H II region were determined by the approximation expressions defining their dependence on the abundance of O/H (see [15]). These expressions were obtained from the results of [8, 30]. To determine the abundances of C/H, Mg/H, Si/H and Cl/H in the 3rd and 4th components we adopted as basis the abundances of the gas within H II region adopted at the Meudon and Lexington meetings [4, 5, 22] for the calculation of photoionization models of the standard H II region. For each model, the abundances of C/H, Mg/H, Si/H and Cl/H were obtained as product of corresponding adopted basis composition and fixed gas metallicity factor, determined as ratio of oxygen abundances at current metallicity to the one, adopted as basis abundance correspondingly.

The chemical abundances inside component 2 were determined by averaging over mass of ones in components 1 and 3, because of matter evaporation at the bound between components 2 and 3 (see below and [31]).

Code `Cloudy 08.00` also makes possible to take into account the dust grains presence during the photoionization modelling. Dust was taken into account in photoionization modelling of the 3rd and 4th components. The distribution of sizes of dust particles was taken from [5, 18]. As in [14, 15], a mixture of silicate and carbonate dusts with basis abundance corresponding to the interstellar medium modelling. Of course, in models this dust abundance was renormalized by dust metallicity factor, determined in the similar way as described above gas metallicity factor.

Thus, we are able to track the evolution of important physical parameters of such complex multicomponent nebular environment as well as the emission line spectra originating within them.

The temperature distribution in the first component (in contrast to our previous works, where we assumed the component temperature to be constant) was calculated in accordance with the model of Chevalier and Clegg [3]:

$$T_1 = 0.0106 \left(\frac{r}{r_0}\right)^{-10/3} \dot{M}_{\rm w}^{1/2} \times \\ \times {L_{\rm w}}^{1/2} {r_0}^{-2}\,[{\rm K}] \quad (r_0 = 1\,{\rm pc}).$$

Taking into account the data from [31], the velocity in the first component corresponds to the stellar superwind velocity $v_1 = v_{\rm w}$ [km/s].

The number density in the 1st component was calculated in accordance with data from [2, 3]:

$$n_1 = \frac{\dot{M}_{\rm w}}{4\pi r^2 m_{\rm H} v_{\rm w} ChF_{in}}\,[{\rm cm}^{-3}],$$

where r is the distance from the starburst, $m_{\rm H}$ is the mass of a hydrogen atom, and ChF_{in} is the total abundance of all chemical elements relative to hydrogen for the internal components [15].

The 2nd component is limited by the inner and outer radii r_1 and r_2 that were determined according to expressions from [31]. Using these radii as well as n_1 distribution and M_{sb} the mass of the 1st component M_1 was determined at required ages. The physical conditions along the 2nd component radius, in accordance with [1, 31], are given by the solution of equations of continuity and energy transfer taking into account the thermal conductivity. The boundary conditions under which this system was solved numerically and the solution itself (distribution of dimensionless electron temperature τ and expansion rate u over the dimensionless radial coordinate ξ) can be found in our previous papers [14, 15]. Thus, by multiplying the τ and u values by the relevant factors, taken from [1, 31], we obtained the expressions for the distributions of the electron temperature T_2, the rates of expansion v_2, and density n_2 in the second component as a function of the grid free parameters:

$$T_2 = TF \cdot \tau\,[\mathrm{K}],$$

$$TF = 9.65 \cdot 10^5 \left[n_0^{2/35} \left(\dot{M}_6 \cdot v_{2000}^2 \right)^{8/35} t_6^{-6/35} \right],$$

$$v_2 = VF \cdot u\,[\mathrm{cm/s}], VF = \frac{3}{5} \cdot \frac{r_2}{t},$$

$$n_2 = DF \cdot (1/\tau)[\mathrm{cm}^{-3}] \text{ (if the process is isobaric)},$$

$$DF = \frac{M_2}{\frac{4}{3}\pi ChF_{mix} m_{\mathrm{H}} ({R_2}^3 - {R_1}^3)},$$

$$\dot{M}_6 = \frac{\dot{M}_{\mathrm{w}}}{10^{-6}\ M_\odot/\mathrm{yr}}, v_{2000} = \frac{v_{\mathrm{w}}}{2000\ \mathrm{km/s}}, t_6 = \frac{t}{10^6\ \mathrm{yr}}.$$

where ChF_{mix} is the total abundance of all chemical elements relative to hydrogen in the second component. The abundance for each of chemical elements in this component was determined like mixture of chemical abundances within the 1st and 3rd component averaged over mass using the corresponding expression:

$$\left(\frac{\mathrm{A}}{\mathrm{H}}\right)_{mix} = \left(\frac{\mathrm{A}}{\mathrm{H}}\right)_1 \left(1 + \frac{\mathrm{H}_3}{\mathrm{H}_1}\right)^{-1} + \left(\frac{\mathrm{A}}{\mathrm{H}}\right)_3 \left(1 + \frac{\mathrm{H}_1}{\mathrm{H}_3}\right)^{-1}$$

(index 1 and 3 indicates abundances of chemical elements of the first and of the third components, respectively).

Mass of the 2nd component was determined as follows:

$$M_2 = (M_{sb} - M_1) + \int_0^{age} \dot{M}_b \mathrm{d}t,$$

where $\dot{M}_b$ – rate of the gas mass evaporation from the 3rd component into the second one (see below).

For each of specific models, these dependencies were re-scaled for the corresponding values of r_1 and r_2.

The electron temperature in the 3rd and 4th components was determined during the photoionization modelling using the energy balance equation for photoionization modelling.

The gas density n_3 in dense thin layer (component 3) was determined from the isobaric conditions at the contact discontinuity between the 2nd and 3rd components. The outer radius of the 3rd component was determined during photoionization modelling using the known mass of the third component, determined as follows:

$$M_3 = \frac{4\pi}{3} ChF_{out} m_{\mathrm{H}} n_0 r_2^3 - \int_0^{age} \dot{M}_b \mathrm{d}t.$$

It is mass of gas compressed by the outer shock (here, ChF_{out} is the same total abundance of all chemical elements relative to hydrogen but for the external components) minus the mass of gas evaporated from the 3rd component into the 2nd one [2]:

$$\dot{M}_b = \frac{16}{25} \frac{\mu}{k} C {T_b}^{5/2} R_2,$$

where the central temperature in second component:

$$T_b = 1.6 \cdot 10^6 \left[{n_0}^{2/35} (\dot{M}_6 \cdot v_{2000})^{8/35} {t_6}^{-6/35} \right] [\mathrm{K}].$$

In any way, the contribution of this process in the formation of the mass of the 3rd component is insignificant. The calculation of our model was stopped in the case of the pressure balance at the boundary of the 3rd and 4th components. The outer radius of the 3rd component and the age at which it occurs are called stagnation radius and age correspondingly. Simultaneously, the bubble expansion stops, and later, probably, the third component is fragmented with the further decay of the adopted SWR structure due to the hydrodynamic instabilities. We do not consider in our simulation these processes, therefore we stop calculation for each evolutionary sequence of models at stagnation age.

RESULTS, THEIR ANALYSIS AND CONCLUSIONS

Thus, we calculated MPhMs grid taking into account the internal structure of low-metallicity H II regions and its evolution formed by superwind from central star-forming region. Such models can explain 1) the origin of He II and [Ne V] emission lines [13], observed in spectra of H II regions in some BCDGs [30], as well as 2) the transformation of Lyc-spectra from stars during radiative transfer of the ionizing quanta through superwind bubble components [16, 19]. Therefore we have concluded that

MPhMs describe ionization structure of H II regions in more correct way than ordinary photoionization models. Consequently, the ICFs obtained using the results of MPhMs should be more correct.

We have decided to investigate 1) how new ICFs, derived on the base of ionic abundances calculated in MPhMs grid, change the determination of chemical abundances in low-metallicity H II regions in BCDGs and 2) whether these new ICFs have significant impact on determination of the primordial helium abundance and its enrichment during stellar chemical evolution of matter in the Universe.

For this purpose we selected from the all of MPhMs the ones reproducing the observational data in the best way. We used the Pilyugin compilation [23–25] of the relative intensities of strong emission lines in observed spectra of H II regions in spiral and irregular galaxies, in which at least one auroral line was detected, as the observational data, which made it possible to determine the chemical composition by the T_e-method.

Free parameters of these models are characterized by the values $t = 1 \ldots 10$ Myr, in the range of metallicities corresponding to $12 + \lg(\mathrm{O/H}) = 7.1 \ldots 8.2$.

In Fig. 2 the comparison of the following strong emission line intensities obtained from selected MPhMs with ones obtained during spectroscopic observations are shown. The line intensities are defined as follows:

$$R_2 = ([\mathrm{O\,II}]\,3727 + [\mathrm{O\,II}]\,3729)/\mathrm{H}_\beta,$$

$$R_3 = ([\mathrm{O\,III}]\,4959 + [\mathrm{O\,III}]\,5007)/\mathrm{H}_\beta,$$

$$N_2 = ([\mathrm{N\,II}]\,6548 + [[\mathrm{N\,II}]\,6584)/\mathrm{H}_\beta,$$

$$S_2 = ([\mathrm{S\,II}]\,6717 + [\mathrm{S\,II}]\,6731)/\mathrm{H}_\beta.$$

The ionic abundances $\mathrm{A}^{+i}/\mathrm{H}^+$, obtained as result of averaging of ones, calculated in MPhMs, over volumes of outer bubble component and outer H II region (these components emit most of quanta in observed emission lines) and weighted over the electron density in these components, as well as the chemical compositions A/H, adopted in MPhMs, were used to determine the new expressions for ICFs in the following way:

$$\log[(\mathrm{A}^{+i}/\mathrm{H}^+)/(\mathrm{A/H})] = f(x),$$

$$x = X^{+k+1}/X^{+k},$$

$$f(x) = \sum_{n=0}^{4} C_n x^n,$$

$$\mathrm{ICF}(x) = 10^{-f(x)},$$

where C_n – coefficients of a polynomial, and $f(x)$ – approximation function that defines the ICFs. Thus, if $(\mathrm{A}^{+i}/\mathrm{H}^+)_{diagn}$ and $X^{+k+1}_{diagn}/X^{+k}_{diagn}$ are the ionic abundances obtained as result of observed emission line spectra diagnostic of some low-metallicity H II region, then relative chemical abundance of element A in this object can be determined as follows:

$$\frac{\mathrm{A}}{\mathrm{H}} = \mathrm{ICF}(X^{+k+1}_{diagn}/X^{+k}_{diagn}) \cdot \left(\frac{\mathrm{A}^{+i}}{\mathrm{H}^+}\right)_{diagn}.$$

For an example, in Fig. 3 we show the corresponding dependencies between ionic abundances and chemical ones for He/H and O/H determination. It can be seen that ICFs for He/H determination must be taken into account, while ones for O/H can be neglected, because of small value of $f(x)$ and corresponding ICFs are very close to unity over all interval of x. The same situation occurs in the case of all ICFs based on sum of ionic abundances $(\mathrm{O}^+ + \mathrm{O}^{++})/\mathrm{H}^+$.

The table containing the coefficients $C_0 - C_4$ of a polynomial approximation formula for $f(x)$ determination, the corresponding standard deviations (SD) as well as the ratios $(\mathrm{A/H})_{calc}/(\mathrm{A/H})_{mod}$ of the chemical abundance obtained using corresponding ICF for each of the MPhMs to the one assumed in model, which were averaged over MPhMs grid, is available on the web-site[1]. The figures like 3, used for derivation of our ICFs (functions $f(x)$), also can be found in this web-site.

The chemical compositions of He/H and heavy elements calculated using our ICFs were applied for the helium abundance determination by mass Y and its dependencies on Z and O/H:

$$Y = \frac{4y(1-Z)}{1+4y}, \quad Z = \frac{Z_a}{1 + 4\frac{\mathrm{He}}{\mathrm{H}} + Z_a},$$

where

$$Z_a = 14\frac{\mathrm{N}}{\mathrm{H}} + 16\frac{\mathrm{O}}{\mathrm{H}} + 20\frac{\mathrm{Ne}}{\mathrm{H}} + 32\frac{\mathrm{S}}{\mathrm{H}} + 40\frac{\mathrm{Ar}}{\mathrm{H}},$$

$$y \equiv \mathrm{He/H} = (y^+ + y^{++}) \cdot \mathrm{ICF}(x),$$

$$x = \mathrm{O}^{2+}/\mathrm{O}^+ \text{ or } \mathrm{Ar}^{3+}/\mathrm{Ar}^{2+},$$

$$y^+ = \mathrm{He}^+/\mathrm{H}^+, \quad y^{++} = \mathrm{He}^{++}/\mathrm{H}^+.$$

In general, we have chosen 88 H II regions in BCDG from papers [8–12]. So, we have applied our new ICFs to the relative ionic abundances from these papers and obtained the chemical abundances of heavy elements and helium one using our new ICFs obtained in descibed above way. The range of X^{+k+1}/X^{+k} from our selected models allowed us to obtain the chemical abundances in 83 objects from mentioned 88.

[1] http://physics.lnu.edu.ua/wp-content/uploads/LM_ICFs.pdf

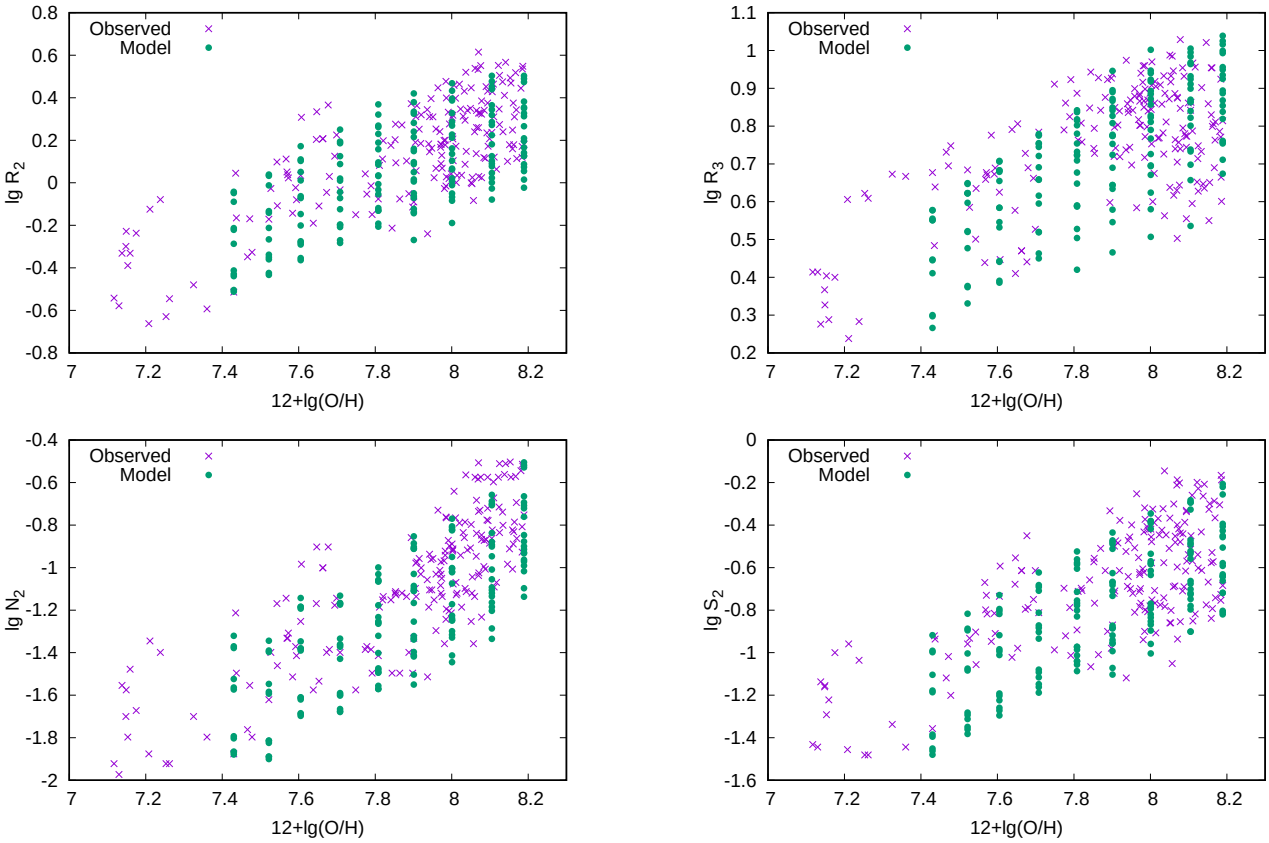

Fig. 2: Comparison of model (circles) and observed (crosses) values of the relative intensities of strong emission lines as functions of $12 + \log(\mathrm{O/H})$.

In Fig. 4 the comparisons of our abundances of He/H as well as O/H with ones from [12] are shown. We did not show the error bars in figure for He/H comparison with purpose to see the differences between results more clearly. It can be seen that most of He/H values obtained using our ICFs are slightly, but systematically, shifted down in comparison with results obtained by [12].Nevertheless, it should be also noticed that He/H abundances coincide within error bars. On the other hand, the O/H abundances coincide very good only for lowest metallicity objects, while with increasing of metallicity our values for O/H are systematically lower comparing to ones from [12].

From our models we obtained the following dependence $Z - \mathrm{O/H}$: $Z = 15.45 \cdot \mathrm{O/H} - 5.48 \cdot 10^{-6}$.

Using our chemical abundances we obtained the dependencies $Y - Z$ and $Y - \mathrm{O/H}$. The dependencies $Y - Z$ and $Y - \mathrm{O/H}$ and their linear approximations are shown in Fig. 5. It can be seen that we obtained the following values of primordial helium abundance: $Y_p = 0.2495 \pm 0.0014$ for $Y - Z$ dependence and $Y_p = 0.2495 \pm 0.0013$ for $Y - \mathrm{O/H}$ one. The derived values of helium enrichment during stellar chemical evolution of matter are $\mathrm{d}Y/\mathrm{d}Z = 3.43 \pm 0.77$ and $\mathrm{d}Y/\mathrm{d(O/H)} = 53.43 \pm 11.69$. Values of Y_p and $\mathrm{d}Y/\mathrm{d(O/H)}$ coincide within error bars with ones obtained by Izotov & Thuan [12] ($Y_p = 0.2516 \pm 0.0011$, $\mathrm{d}Y/\mathrm{d(O/H)} = 40 \pm 7$), but slope $\mathrm{d}Y/\mathrm{d}Z$ in this work is slightly higher than one obtained in [12] ($\mathrm{d}Y/\mathrm{d}Z = 2.19 \pm 0.39$).

Thus, it can be concluded that more precise models of H II regions, which take into account the internal structure of these objects and its evolution, lead to ICFs that slightly decrease the helium abundance. That, consequently, leads to slight decreasing of the primordial helium abundance and to higher values of its enrichment. It is important, because primordial helium abundance, obtained by Izotov et al. after 2007, is significantly higher than predicted by standard big bang nucleosynthesis theory. Thus, the question arises: whether inconsistency between above data on primordial helium can be explained by incorrect ICFs for He? To answer this question it is necessary to calculate the grid of MPhMs based on the precise chemodynamical simulations of H II regions in BCDGs. And that is what we plan to do in our future works.

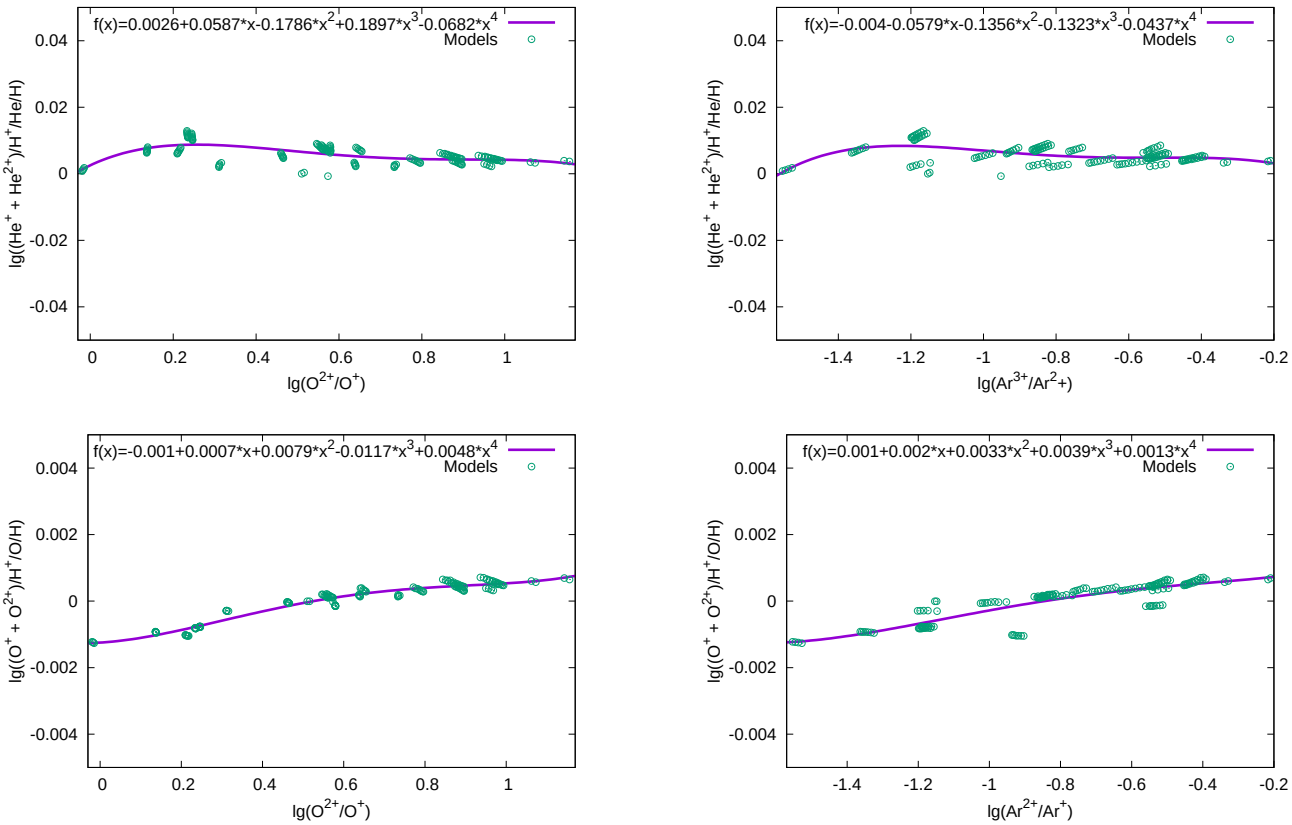

Fig. 3: The examples of derivation of ICFs for He/H and O/H determination in low-metallicity H II regions.

ACKNOWLEDGEMENT

This work was partly supported by the Projects ФФ-63Нр (№ 0117U007190) and ФА-71Ф (№ 0118U003607) from the Ministry of Education and Science of Ukraine.

REFERENCES

[1] Bochkarev N. G., Zhekov S. A. 1990, AZh, 67, 274.
[2] Castor J., McCray R., Weaver R. et al. 1975, ApJ, 200, L107.
[3] Chevalier R. A., Clegg A. W. 1985, Nature, 317, 44.
[4] Ferland G., Binette L., Contini M. et al., 1995, *'The Analysis of Emission Lines'*, Cambridge University Press.
[5] Ferland G. J., 2008, *'Hazy, a Brief Introduction to Cloudy'*, University of Kentucky[2].
[6] Holovatyi V. V., Melekh B. Ya. 2002, Kinematika i Fizika Nebesnykh Tel, 18/4, 362.
[7] Holovatyy V. V., Melekh B. Ya. 2002, Astron. Rep., 46, 779.
[8] Izotov Yu. I., Thuan T. X., Lipovetsky V. A. 1994, ApJ, 435, 647.
[9] Izotov Yu. I., Thuan T. X., Lipovetsky V. A. 1997, ApJS, 108, 1.
[10] Izotov Yu. I., Thuan T. X. 1998, ApJ, 500, 188.
[11] Izotov Yu. I., Thuan T. X. 2004, ApJ, 602, 200.
[12] Izotov Yu. I., Thuan T. X. 2007, ApJ, 662, 15.
[13] Koshmak I. O., Melekh B. Ya. 2013, Kinematics Phys. Celestial Bodies, 29, 257.
[14] Koshmak I. O., Melekh B. Ya. 2013, J. Phys. Studies, 17, 4901.
[15] Koshmak I. O., Melekh B. Ya. 2014, Kinematics Phys. Celestial Bodies, 30, 70.
[16] Kozel R. V., Melekh B. Ya. 2009, in *'YSC'16 Proc. of Contributed Papers'*, ed. Choliy V. Ya., Ivashchenko G., 37.
[17] Leitherer C., Schaerer D., Goaldader J. D. et al. 1999, ApJS, 123, 3.
[18] Mathis J. S., Rumpl W., Nordsieck K. H. 1977, ApJ, 217, 425.
[19] Melekh B. Ya., Koshmak I. O., Kozel R. V. 2011, J. Phys. Studies, 15, 3901.
[20] Melekh B. Ya., Pilyugin L. S., Korytko R. I. 2012, Kinematics Phys. Celestial Bodies 28, 189.
[21] Pauldrach A. W. A., Hoffmann T. L., & Lennon M. 2001, A&A, 375, 161.

[2] http://www.nublado.org

[22] Péquignot D. 1986, in *Proceedings of Workshop on Model nebulae*, Publication de l'Observatoire de Meudon, Paris.
[23] Pilyugin L. S., Vílchez J. M., Thuan T. X. 2010, ApJ, 720, 1738.
[24] Pilyugin L. S., Grebel E. K., Mattsson L. 2012, MNRAS, 424, 2316.
[25] Pilyugin L. S., Grebel E. K., Kniazev A. Y. 2014, AJ, 147, 131.
[26] Schaerer D., de Koter A., Schmutz W., & Maeder A. 1996, A&A, 310, 837.
[27] Schaerer D., de Koter A., Schmutz W., & Maeder A. 1996, A&A, 312, 475.
[28] Stasinska G. 1990, A&AS, 83, 501.
[29] Tarter C. B. 1967, Ph. D. Thesis, Cornell University, 28-10, 3983.
[30] Thuan T. X., Izotov Yu. I. 2005, ApJS, 161, 240.
[31] Weaver R., McCray R., Castor J., Shapiro P., Moore R. 1977, ApJ, 218, 377.

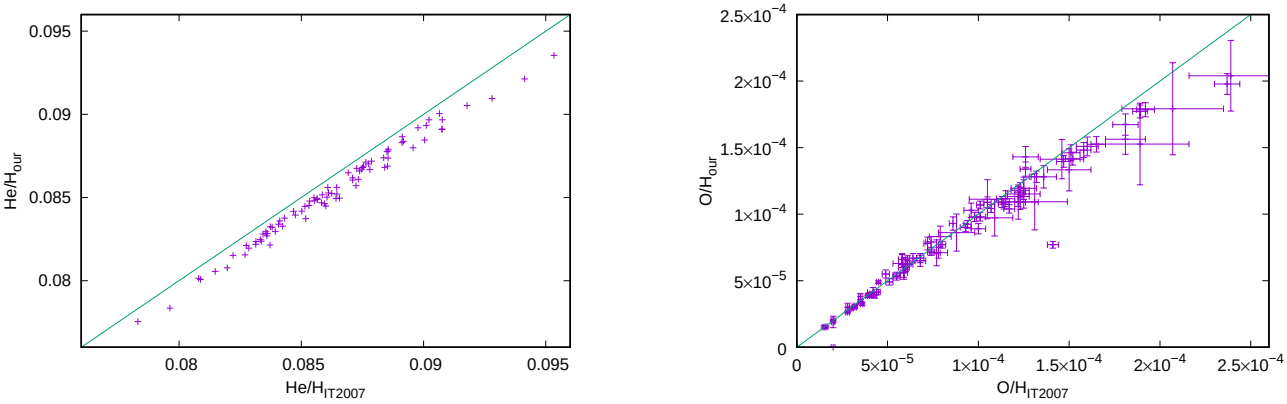

Fig. 4: Comparison of obtained He/H and O/H abundances in H II regions of BCDGs with ones from [12].

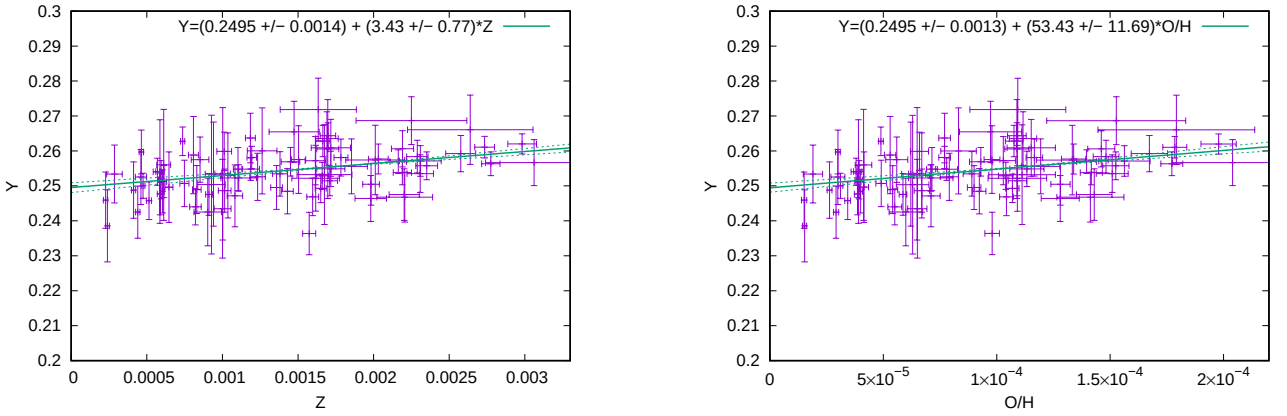

Fig. 5: Determination of the primordial helium abundance and its stellar enrichment.